An Underactuated PASA Finger Capable of Perfectly Linear Motion With Compensatory Displacement

Eric Zheng[1]

Department of Mechanical Engineering,
Tsinghua University,
Beijing 100084, China
e-mail: erzheng@ctemc.org

Wenzeng Zhang[2]

Mem. ASME
Department of Mechanical Engineering,
Tsinghua University,
Beijing 100084, China
e-mail: wenzeng@tsinghua.edu.cn

This paper presents a novel design for a robotic end effector. In particular, the design features a multifingered underactuated gripper capable of performing parallel and self-adaptive (PASA) grasping. The unique use of an eccentric cam fixed to a modified four-bar linkage mechanism allows the finger to compensate for the typical gap distance found during parallel pinching, improving the ability to grasp objects against surfaces and in tight spaces. A static analysis is performed on the design to determine the equilibrium conditions necessary for a successful grasp using this design in both the PASA modes. The mechanics of a four-bar mechanism are used to determine the grasp velocity and positioning of the hand in both grasp modes. Experimental results with a finger prototype confirm the desired closing trajectory.
[DOI: 10.1115/1.4041786]

1 Introduction

As robots move to new, highly unpredictable environments such as homes or outdoors, the demands placed on their grasping abilities become increasingly complex. Grasping is a difficult task, and the sophistication of the hardware involved has become a major hurdle in robotics [1]. Traditional dexterous robotic hands, such as the Utah/M.I.T. hand [2], the Stanford/JPL hand [3], the Robonaut hand [4], the Shadow Hand [5], and the DLR hand [6], have required large numbers of actuators, leading to elaborate control schemes involving multilayered computer algorithms [7] and complex actuation and simulation software [8]. In many cases, such hands are impractical or inefficient due to the intensive hardware and software requirements: a traditional fully actuated dexterous hand with only three fingers must have at least nine actuators [1], not counting additional fingers or redundant degrees-of-freedom. Additionally, fully actuated hands can be costly and prone to hardware failure [9]. As an example, weight restrictions for usability of prosthetic hands make fully actuated standalone prosthetic hands very difficult to make with current technology [10]. The need to realize a wide variety of complicated grasps while maintaining a relatively simple control scheme and low weight has led to the recent development of underactuated fingers that are mechanically intelligent; examples include the SDM [11] and the SARAH [12] hands. Such fingers require fewer actuators than the number of degrees-of-freedom that they

possess, relying instead on self-adaptive mechanical designs incorporating passively compliant elements. This allows the hand to perform a multistage grasp, with preloaded springs used to passively control the hand motion until contact with the object being grasped, effectively enabling the hand to respond to the environment and automatically select the best grasp to perform [13].

For a conventional underactuated multifingered robotic hand, there are three primary modes of grasping: parallel, coupled, and self-adaptive. The grasp modes relevant to this paper, the parallel and self-adaptive (PASA) grasps, are shown in Fig. 1. Many modern hands focus on the combination of these types of grasps; examples include the PASA and coupled and self-adaptive grasping schemes [14]. Several such hands have already been created using a variety of mechanisms, including designs using tendons [15], linkages [16–18], and belt drives [19,20]. However, an issue exists with most current designs for PASA hands: as the fingers close, they effectively become lower in height, creating a gap. This is the result of the circular motion of the fingertip during parallel grasping: as shown in Fig. 2, a circularly parallel finger always creates a gap distance Δs as it moves an angle θ to the left or right of its upright position. The existence of a gap distance makes it difficult to pick up small items that rest against a surface, a task commonly encountered when picking up items from a table. Given this gap distance, the finger's own motion will either miss a small object or interfere with the surface, necessitating a more complex grasping scheme.

There are already several hand designs that can perform a linearly parallel grasp, thus avoiding this problem entirely. The most basic is the industrial parallel-jaw gripper, which cannot perform an encompassing grasp. Better examples of linearly parallel grippers include the approaches given by Gao et al. [21,22] and Birglen [23], in which the entire finger moves linearly with respect to the base until it is deformed by contact with an object. This approach combines many of the merits of the simple gripper with self-adaptability, but this sliding motion precludes any sort of dexterous manipulation and prohibits the hand from extending itself to a wider angle to accommodate larger objects, since linear motion is dependent upon maintaining a fixed angle with the base. More common is the circular PASA finger, but with current implementations, such a linear grasp can only be realized using wrist movement, increasing the control complexity, requiring a visual sensor, and wasting the primary benefit of an underactuated design: simplicity. In this paper, we, therefore, propose a novel modification to the circularly parallel scheme to allow for the advantageous linear fingertip motion during parallel grasping while maintaining the traditional, human-like circular motion of the overall hand.
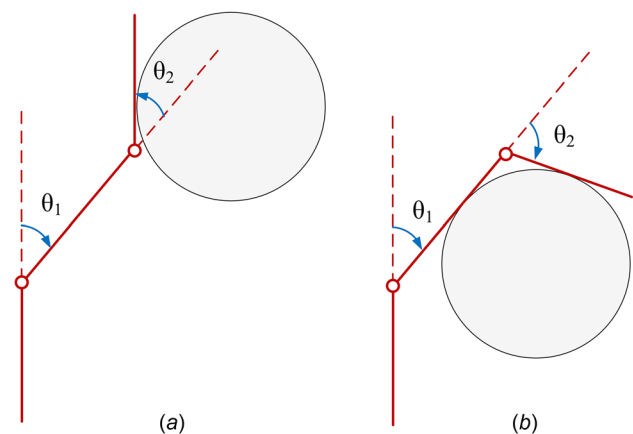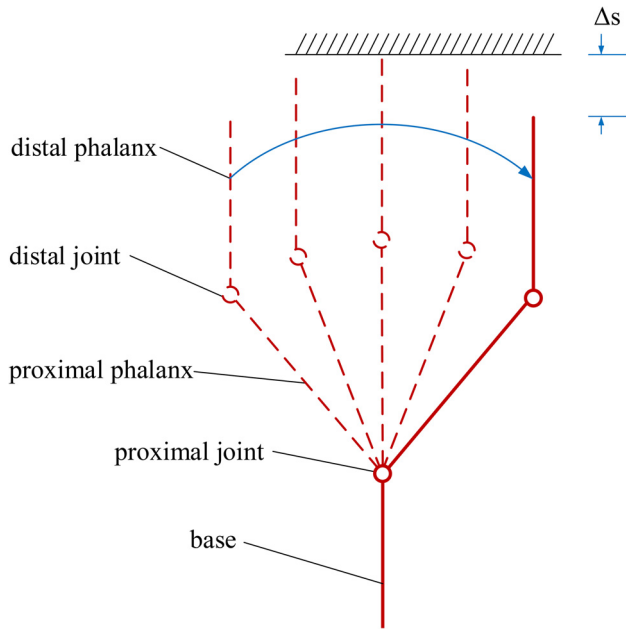

Fig. 1 Phalanx positioning during (*a*) parallel (pinching) and (*b*) self-adaptive (encompassing) modes, showing proximal and distal joint shaft angles θ_1 and θ_2. In the parallel phase, $\theta_1 = \theta_2$ to keep the distal phalanx parallel to its initial orientation.

Fig. 2 Parallel pinching with circular motion and resulting gap distance $\Delta s = L_1 - L_1 \cos\theta$, where L_1 is the length of the proximal phalanx, and θ is the angle from the upright position

In order to maintain linear fingertip travel with a circularly parallel design, the finger length must vary with the angle of rotation; we term the exact extension or retraction needed to compensate for the gap of the "compensatory displacement." It is not desirable to accomplish this through the introduction of another actuator or feedback loop into the control scheme, since this would again defeat the purpose of an underactuated finger design. Many obvious designs, such as the rack and pinion, can provide only

Table 1 Link lengths used in the design, analysis, and experiments found in this paper. Link labels refer to Fig. 3(c).

Link	Length (mm)
L_{AC}	30
$L_{BC} = L_{DE}$	15
$L_{CE} = L_{BD}$	40
L_{AD}	42.72

an approximation of the true gap distance, meaning that they do not scale up well and are not suitable for high-precision environments. Although perfectly linear motion is certainly mechanically possible with a larger, more complex mechanism like a Peaucellier–Lipkin linkage [24], mathematical and mechanical simplicity are desirable to ensure robust, reliable motion. In order to achieve such motion, the design in this paper uses an eccentric circular cam, which lifts a follower whose motion is precisely proportional to the required compensatory displacement. This has the advantage of being compact, simple, and, as our analytical and experimental results demonstrate, effectively realizes both pinching and encompassing grasp modes.

2 Finger Design

The finger consists of three segments—a base, proximal phalanx, and distal phalanx—connected by the proximal and distal interphalangeal joints. This section discusses the motion of the three segments during the parallel and self-adaptive grasp phases. The overall construction is shown in Fig. 3, with link dimensions given in Table 1; the mechanisms are further illustrated in Fig. 4.

2.1 Parallel Pinching. In the base, the motor torque is transmitted to AC, causing it to turn. Due to the spring, BC remains effectively stationary at this time. This causes the entire finger to move forward while the parallelogram geometry of the four-bar
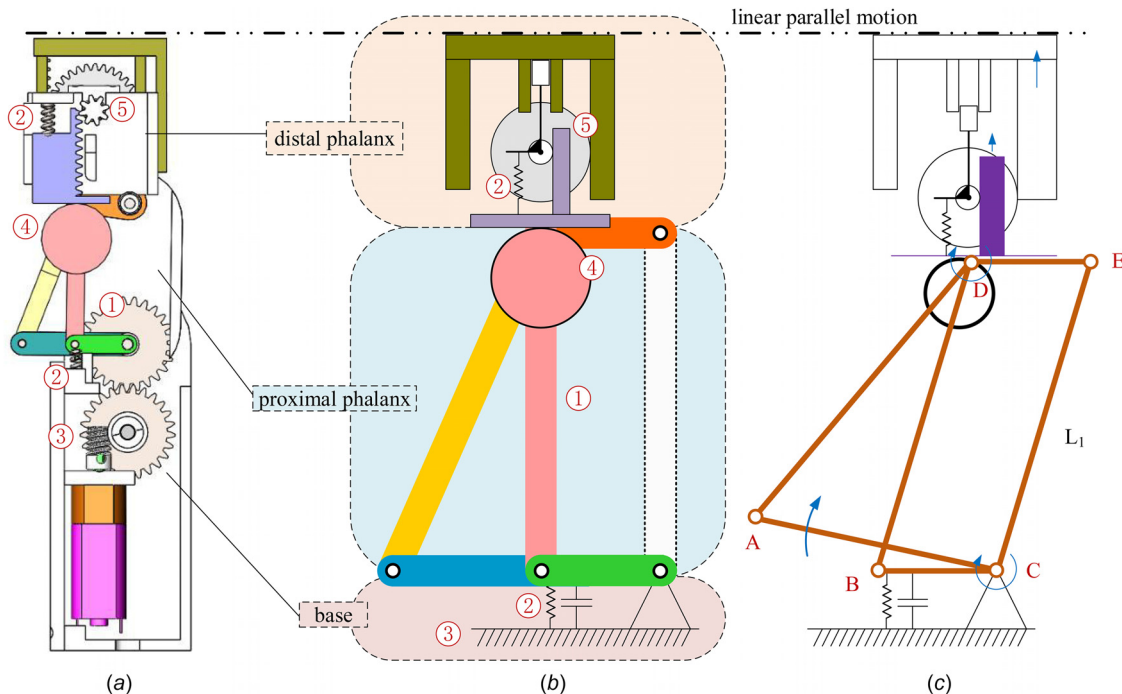
Fig. 3 (a) Drawing of finger design made by CAD software and (b) diagram of the linkage mechanism, labeled by components: (1) linkage mechanism, (2) spring and mechanical limit, (3) base, (4) cam and follower, and (5) concentric gears and gear racks. (c) finger schematic during parallel pinching, with the linkage elements labeled.
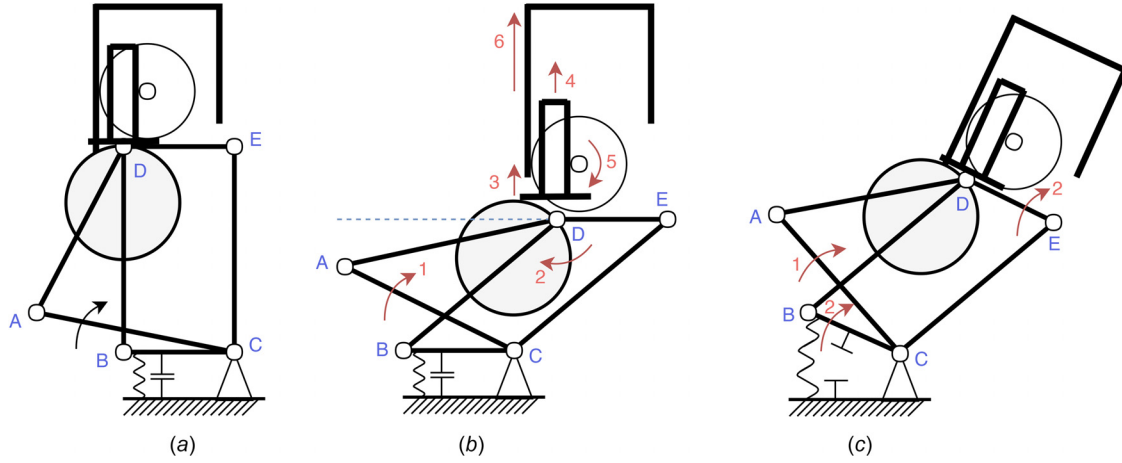
Fig. 4 Demonstration of the finger pose in the (*a*) upright, (*b*) parallel, and (*c*) self-adaptive cases. In the (*b*) parallel case, when the finger is actuated (1), the cam rotates (2), rising with respect to the finger (3) and lifting the follower (4). This turns the gears (5), thus extending the distal phalanx (6). In the (*c*) self-adaptive case, CE is effectively grounded by contact with the object, so when the finger is actuated (1), links BC and DE turn (2) against the spring.

mechanism BCDE forces the distal phalanx, mounted on DE, to stay parallel to its initial position. Because the cam is fixed to BD, they rotate together; as the proximal phalanx rotates an angle θ, the cam rotates an apparent angle θ with respect to DE about point D.

As the cam revolves about a point on its circumference, it lifts a flat-faced follower. When the cam of radius r has spun an angle θ corresponding to the proximal shaft angle, the follower travel is given by the distance $r - r\cos\theta$. A concentric gear system is then used to move a slider $\Delta h = p(r - r\cos\theta)$, where p is the ratio between the gear diameters. If p is set correctly, $\Delta h = \Delta s$ from Fig. 2.

Gravity alone cannot maintain contact between the follower and the cam profile, since the follower may be positioned beneath the cam in certain orientations. Instead, a spring with low stiffness is used to press the follower against the cam; it is placed near the center of the follower to reduce the jamming moment.

2.2 Self-Adaptive Grasping. If the finger encounters the object at the proximal phalanx during the parallel motion, it will automatically switch to self-adaptive mode. The motor still rotates link AC, but because CE is now immobilized by the object, link BC is forced to move against the spring. This allows the distal phalanx, fixed to DE, to rotate toward the object until it comes into contact. During this motion, the angle between links BD and DE changes again, causing the cam to rotate with respect to the distal phalanx. This has the effect of shortening and lengthening the distal phalanx; however, in self-adaptive mode, this does not affect the finger's grasping ability.

3 Grasp Analysis

This section analyzes the finger's grasp characteristics, especially the normal forces acting on each phalanx during contact with the object. When the grasp is complete, the hand is in static equilibrium; for a successful grasp, the contact force between the finger and the object must be positive. In this analysis, we define the following values: contact forces F_1 and F_2; object contact distances h_1 and h_2 from the interphalangeal joints; motor torque τ_M; moment arm h_{s1} and spring force F_{s1} on link BC; moment arm h_{s2} and spring force F_{s2} on the cam follower; proximal and distal joint angles θ_1 and θ_2; proximal phalanx length L_1; cam radius r; and spring constants k_1 and k_2. These parameters are listed in Table 2 and shown in Fig. 5.

3.1 Kinematic Analysis of Grasp Velocity. This paper puts forward an interesting analysis of the grasp velocity. Such an analysis may be relevant for applications which require a high degree of precision and timing, such as grasping a small, moving object. For a finger actuated by a motor angular velocity ω_M, this section determines the resulting ω_p and ω_s, the angular velocities of the proximal and distal phalanges during the parallel and self-adaptive phases, respectively.

The input angle ϕ of link AC is related to the joint angles θ_1 and θ_2. Rather than modeling the hand with Jacobian and transmission matrices as given by Birglen and Gosselin [25], this section gives a simpler analysis using the known mechanics of a four-bar mechanism. During the parallel and self-adaptive phases, geometric constraints provided by the spring and object cause the six-bar linkage to simplify to two four-bar linkages, an observation made earlier by Gao et al. [22] in a different analysis. During the parallel phase, the grounding of link BC by the spring causes the mechanism to behave as a four-bar linkage ADCB, with input link AC, frame BC, coupler AD, and output BD. Similarly, the grounding of link CE during the self-adaptive phase creates a quadrilateral linkage ACED with input AC, ground CE, coupler AD, and output DE. The relationships between the angle of the common input link AC and the angles of the output links BD and DE can be found by separately solving the constraint equations for the two four-bar linkages.

In general, for input and output angles ϕ and ψ, the constraint equation takes the form, as noted by Belzile and Birglen [26]

$$A(\phi)\cos\psi + B(\phi)\sin\psi + C(\phi) = 0 \qquad (1)$$

Table 2 Design parameters used in grasp analysis and experiments

Parameter	Value	Units
L_1	40	mm
τ_M	500	N·mm
k_1	1	N/mm
k_2	0.5	N/mm
h_{s1}	15	mm
h_{s2}	20	mm
r	10	mm
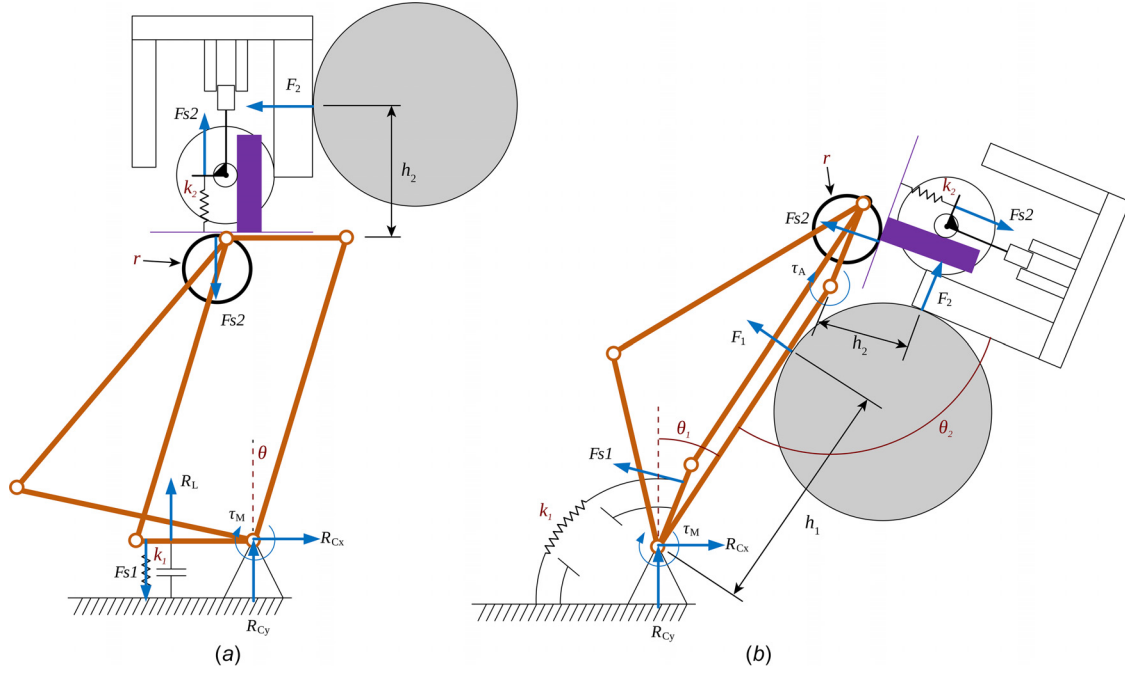
Fig. 5 Dynamic and kinematic quantities referenced in the analyses of the (a) parallel and (b) self-adaptive modes

With

$$A(\phi) = 2bg - 2ab \cos \phi$$
$$B(\phi) = -2ab \sin \phi \qquad (2)$$
$$C(\phi) = a^2 + b^2 + g^2 - h^2 - 2ag \cos \phi$$

where a, b, g, and h are the lengths shown in Fig. 6. Using the method described by Bai and Angeles [27], the output angle ψ is

$$\psi = \tan^{-1}\left(\frac{B}{A}\right) + \cos^{-1}\left(\frac{-C}{\sqrt{A^2 + B^2}}\right) \qquad (3)$$

During the parallel phase, this gives the angular position of the proximal phalanx; during the self-adaptive phase, this gives the angular position of the distal phalanx. Following the analysis of

Fig. 6 Kinematics of a four-bar mechanism, upon which the finger is based. When a and b overlap, the new g' is given by $g' = -g$.

Rothenhofer et al. [28], the time derivative of the constraint equation is then used to determine the speed ratio:

$$\frac{\dot{\phi}}{\dot{\psi}} = \frac{ab \sin(\phi - \psi) + bg \sin \psi}{ab \sin(\phi - \psi) + ag \sin \phi} \qquad (4)$$

Assuming a known motor angular velocity $\omega_M = \dot{\phi}$, the output angular velocity $\dot{\psi}$, corresponding to ω_p and ω_s during the parallel and self-adaptive phases, respectively, can then be calculated according to the geometric design parameters.

From these equations, it is also possible to determine the phalanx positioning (described by θ_1 and θ_2) for any motor angle ϕ, as shown in Fig. 7. Such an analysis may be relevant for practical applications, such as the position control of an underactuated finger using encoder feedback, improving the precision of grasps when dealing with objects of known size and location. Equation (3) can be used to solve ϕ when considering the inversion of the linkage: swapping the input and output links will swap the input and output angles. Letting $\Psi(x)$ represent Eq. (3), ϕ, with respect to its initial orientation parallel to the base, is
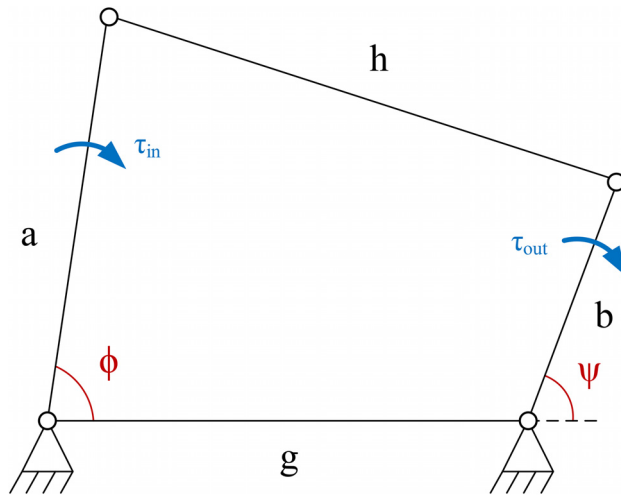
$$\phi = \frac{\pi}{2} - \Psi\left(\theta_2 + \frac{\pi}{2}\right) + \theta_1 \qquad (5)$$

3.2 Static Analysis of Parallel Pinching. During parallel pinching, the proximal phalanx does not contact the object, so $F_1 = 0$. Additionally, for the distal phalanx to remain parallel to its initial orientation, $\theta_1 + \theta_2 = 0$. As the two angles are equal, it is convenient to refer to them both as the angle θ.

Since the spring attached to link BC experiences negligible deformation, F_{s1} is effectively zero. The second spring, pushing on the follower, is compressed, but the resulting torques cancel. Likewise, the reaction forces F_L, R_{Cy}, and R_{Cx} do not affect this analysis and are included in Fig. 5 only for completeness.
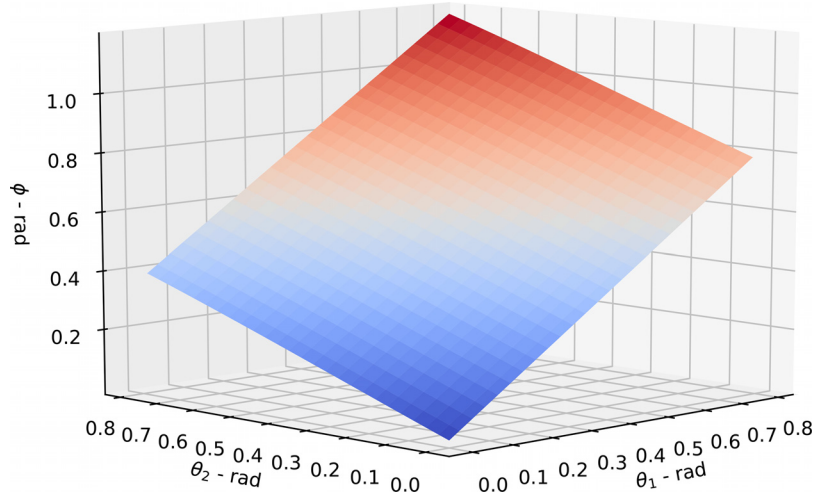
Since the entire finger is in equilibrium, the force F_2, plotted in Fig. 8, is

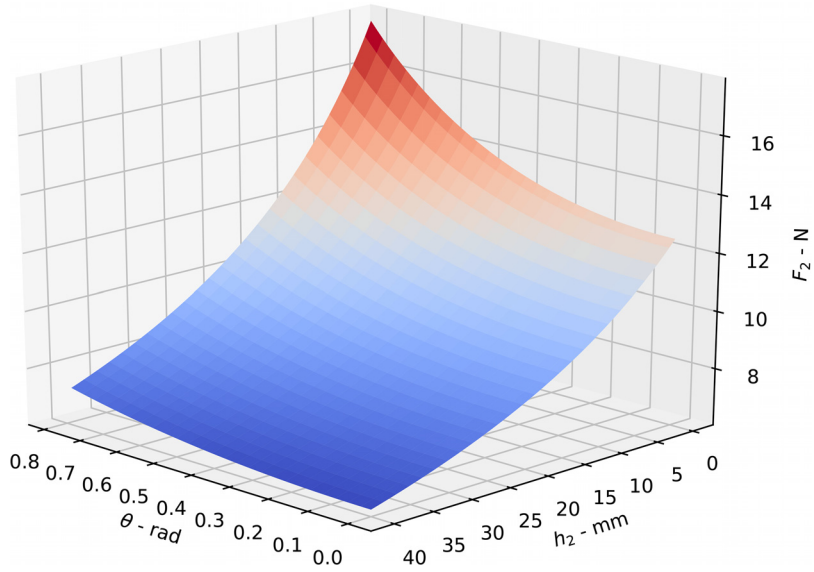$$F_2 = \frac{\tau_M}{L_1 \cos \theta + h_2} \qquad (6)$$

Fig. 7 Required motor input angle ϕ given an arbitrary phalanx positioning described by joint shaft angles θ_1 and θ_2

Fig. 8 Graph of contact force F_2 versus proximal joint shaft angle θ_1 and distal contact distance h_2 in parallel pinching mode

3.3 Static Analysis of Self-Adaptive Grasping. During self-adaptive grasping, there are two contact forces F_1 and F_2, which are functions of the joint angles θ_1 and θ_2, contact distances h_1 and h_2, and the aforementioned design parameters. During this phase, the spring attached to link BC experiences a deformation corresponding to the angle $\theta_1 + \theta_2$. Thus, assuming circular deformation, the spring force and corresponding moment are given by

$$F_{s1} = k_1 h_{s1}(\theta_1 + \theta_2)$$
$$\tau_{s1} = k_1 h_{s1}^2(\theta_1 + \theta_2) \tag{7}$$

The torque generated by F_1 is simply

$$\tau_1 = F_1 h_1 \tag{8}$$

Similarly, the torque generated by F_2 is

$$\tau_2 = F_2(h_2 + L_1 \cos \theta_2) \tag{9}$$

As with before, the torques due to F_{s2} cancel. Equilibrium about C then gives

$$\tau_M = F_1 h_1 + F_2(h_2 + L_1 \cos \theta_2) + \tau_{s1} \tag{10}$$

Additionally, we can consider the balance of torques on the distal phalanx about E to obtain a second equation for static equilibrium. In this situation, F_{s2} is small but not negligible. The distal phalanx has rotated an angle θ_1, becoming collinear with the proximal phalanx, and then another angle θ_2, reaching its final position in contact with the object. The follower travel, and therefore, the compression distance, is then given by $r(1 - \cos \theta_2)$. This force affects the static equilibrium of the distal phalanx by pushing upward on the phalanx.

The actuation torque τ_M on link AC still acts on the distal phalanx, but it acts through the quadrilateral linkage ACED, with the distal phalanx mounted on the output link DE. ACED is additionally constrained by the spring force F_1 acting on link BC, which is transmitted with a 1:1 ratio to link DE due to the symmetric parallelogram linkage BCED. These constraints can be used to relate the contact force F_2 to F_{s2}, τ_M, and F_{s1}.

The mechanics of the four-bar mechanism ACED are examined more closely in the subsection Kinematic Analysis of Grasp
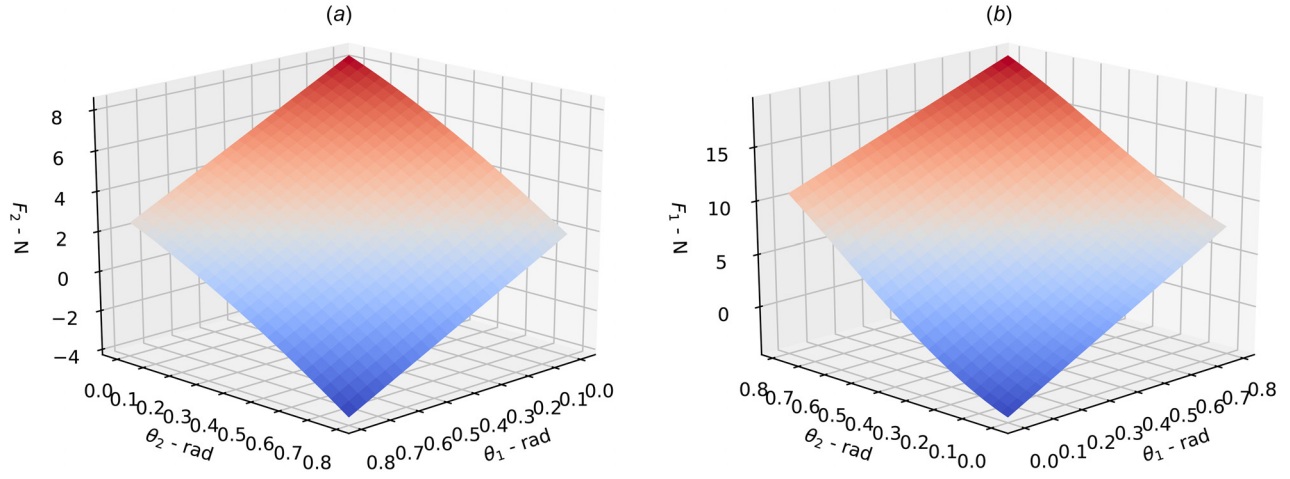
Fig. 9 (*a*) Graph of contact force F_2 versus proximal and distal joint shaft angles θ_1 and θ_2 during self-adaptive mode and (*b*) graph of contact force F_1 versus proximal and distal joint shaft angles θ_1 and θ_2 during self-adaptive mode. In these analyses, h_1 and h_2 are given the average value of 20 mm.

Velocity; here, we reference only the final linkage speed ratio given in Eq. (4). Equating virtual power input and output, the linkage transmission ratio is given by its speed ratio, or $\tau_{in}\dot\phi = \tau_{out}\dot\psi$. The output link DE is directly fixed to the distal phalanx; the torque exerted by the motor through the linkage acting on the distal phalanx about point E is therefore dependent on the speed ratio, which in turn is a function of the geometric configuration of the linkages and the current position of the finger as described by the joint shaft angles θ_1 and θ_2 and the motor input angle ϕ. This allows us to describe the actual torque transmitted to the distal phalanx τ_A as

$$\tau_A = \frac{\tau_M \dot\phi}{\dot\psi} \tag{11}$$

which can be solved using the previously mentioned Eq. (4). Notice that the angles used in the linkage analysis, ϕ and ψ, are measured with respect to the linkage frame CE, which is at an angle $\theta_1 + \pi/2$ to the base of the finger. In practice, it is algebraically easiest to find ϕ and ψ by "reversing" the linkage (swapping the output and input links) and then noting that the input angle (now ψ) is equal to $\theta_2 + \pi/2$ and solving for ϕ using the constraint Eq. (1).

Returning now to the spring force F_{s2}, we examine the force's moment about point E. As noted before, the distal spring during self-adaptive grasping has been deformed a distance $r(1 - \cos\theta_2)$. This creates a spring force pushing at both end2s with magnitude

$$F_{s2} = k_2 r(1 - \cos\theta_2) \tag{12}$$

The spring force F_{s1} directly opposes the torque τ_A applied to link DE. Thus, considering the balance of torques acting on the distal phalanx about point E now gives the equation

$$\tau_A + h_{s2} k_2 r(1 - \cos\theta_2) = F_2 h_2 + \tau_{s1} \tag{13}$$

This can be combined with Eqs. (4), (7), (11), and (12) to solve for the contact force F_2 as

$$F_2 = \frac{\tau_A + h_{s2} k_2 r(1 - \cos\theta_2) - \tau_{s1}}{h_2} \tag{14}$$

This ultimately allows us to solve Eq. (10) to obtain an expression for the contact force F_1

$$F_1 = \frac{\tau_M - F_2(h_2 + L_1 \cos\theta_2) - \tau_{s1}}{h_1} \tag{15}$$

These equations are graphed with the PYTHON MATPLOTLIB software [29] for $h_1 = h_2 = 20$ mm in Fig. 9. As common in underactuated fingers, the decreased number of actuators creates a range of configurations for which the finger cannot exert grasping forces [22]. For this design, this range exists when $F_2 < 0$. It can be seen that this is a relatively small range that occurs around large values of θ_1 and θ_2; this can be improved by increasing actuation torque and properly calibrating the spring constants k_1 and k_2.

4 Experiments

A prototype of a finger was 3D printed from polylactic acid. Although only a single finger prototype was produced, two or three such fingers would be mounted opposite each other on a palm to form a complete hand. The results demonstrate that the finger design is capable of realizing parallel pinching along a straight line as well as self-adaptive grasping. Figure 10 shows a parallel pinch. The extension of the distal phalanx is clearly seen as the finger rotates. Figure 11 shows a self-adaptive grasp in which the finger is seen to clearly envelop the object.

During testing, it was found that the self-adaptive phase had some geometric limitations. The distal joint shaft angle θ_2 was limited; its range depended on the proximal joint shaft angle θ_1. The larger θ_1 became, the smaller the range of θ_2 was. This is consistent with the theoretical simulations shown in Fig. 9(*a*), which shows that as θ_1 increases, the range of θ_2 for which the finger can exert grasp forces at the distal phalanx ($F_2 > 0$) becomes much smaller.

The experiments performed in this paper deal with the closing trajectory of the finger, since this is the most significant part of the design. It would be interesting future work to measure the grasp forces of the prototype to confirm the static analysis.

5 Discussion

A strictly linear parallel motion is desirable for several important applications. As already mentioned, grasping against surfaces, particularly when small objects are involved, is greatly improved with this design. Additionally, being able to execute strictly linear pinching is helpful when executing grasps in constrained spaces, since such spaces may not allow for the wrist movement that a typical circular PASA hand requires.

The applications of the design in this paper seem more suited to industry and pure robotics than to prosthetics and bionics. It has
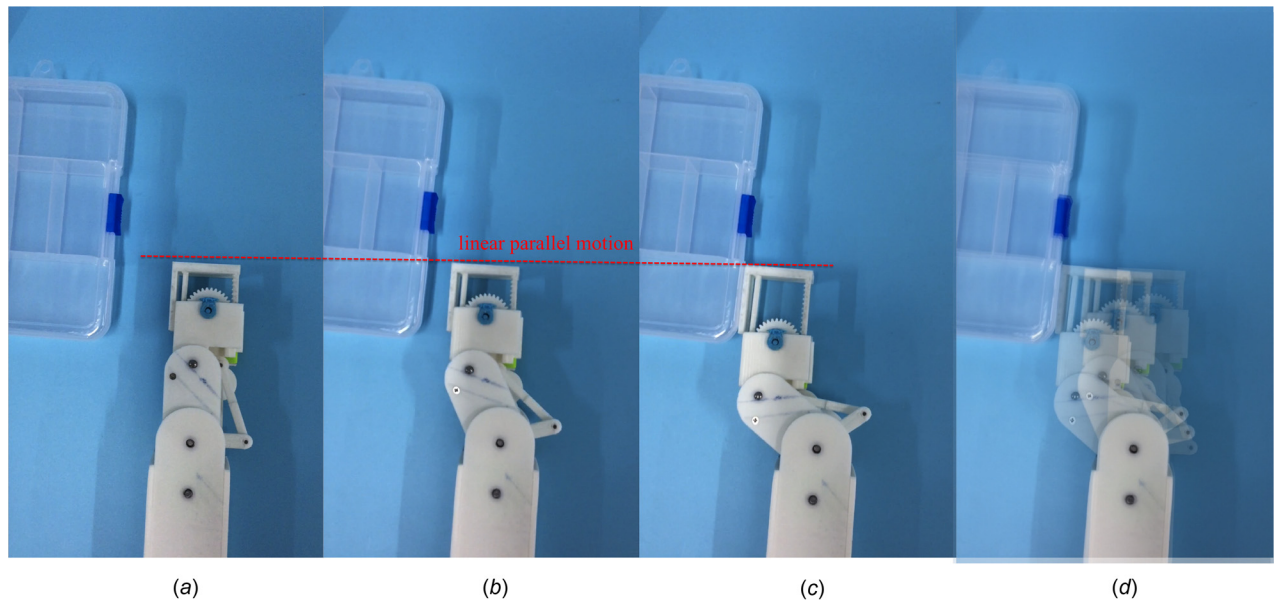
Fig. 10 (*a–c*) The prototype as it completes a parallel grasp and (*d*) composite overlay picture showing the entire parallel pinching process
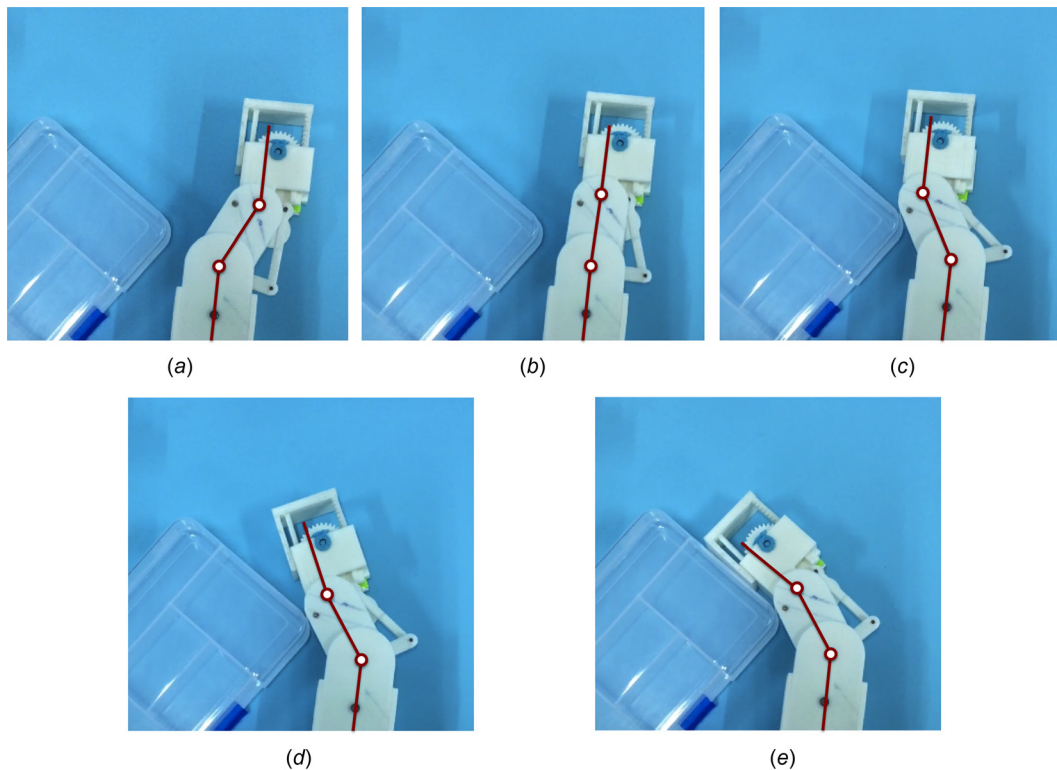
Fig. 11 Finger prototype in an encompassing grasp, with components from Fig. 2 superimposed. In (*a–c*), the finger performs a regular parallel motion, as depicted in Fig. 10. When the proximal phalanx contacts the object in frame (*c*), the finger begins to move self-adaptively. The grasp is complete when both phalanges touch the object, as in frame (*e*).

been noted before [16] that the motions of a PASA hand, while convenient for securely grasping an object using a precision pinch grasp by a robot, do not perfectly mimic the motions of a human hand, which instead tends to grasp using a three-phalanx coupled and self-adaptive approach [14,30]. Additionally, the extension and retraction of the distal phalanx during the grasping process is obviously different from the human hand and could pose a significant obstacle to a human user attempting to use the hand for prosthetic purposes.

Instead, the most likely application for this hand is in robots that interact with humans: the variety of grasp modes would allow the hand to adapt to the variety of objects in a human environment, the mechanical intelligence would ensure robust grasping, and the linear motion would improve the hand's ability to perform common household tasks, especially picking up objects from a table.

The integration of this hand into a more complete robot system, including the control of a manipulator arm housing the end

effector, has not yet been studied. A complete manipulator system would center around a full hand, with of two identical fingers set opposite each other. Other configurations of fingers are also possible; generally, the fingers should be arranged so that they are level with each other, allowing the entire hand to remain at a constant height. In this scheme, each finger is independently actuated; underactuation between fingers, as proposed in Ref. [16], is interesting but not within the scope of this paper, which focuses on the finger design.

Several improvements to this finger could be the subject of future study. The finger's physical parameters, including phalanx lengths, cam radius, and spring placement, were not optimized before construction; optimization using the models in this paper would be interesting. Additionally, the mathematical analysis in this paper covers only normal contact forces; a more complete analysis that accounts for frictional and inertial effects would help to more thoroughly understand the advantages and limitations of the design.

6 Conclusion

In this paper, we developed and examined an underactuated robotic hand. Although such a hand is not new, this paper introduced a novel solution to the gap distance commonly encountered in PASA hand designs. An eccentric cam fixed to the proximal phalanx allows the distal phalanx to automatically extend itself to compensate for this gap while moving in parallel pinching mode. A static analysis of the grasp forces in static equilibrium demonstrates the range of grasp stability; the desired closing trajectory was confirmed by experiments performed with a prototype of a finger. An analysis of the finger mechanics based on the similarities between the complex six-bar mechanism and two simpler four-bar mechanisms yields an approach for computing the angular positions and velocities of the phalanges during parallel and self-adaptive grasping.

References

[1] Bicchi, A., 2000, "Hands for Dexterous Manipulation and Robust Grasping: A Difficult Road Toward Simplicity," IEEE Trans. Rob. Autom., **16**(6), pp. 652–662.
[2] Jacobsen, S., Wood, J., Knutti, D., and Biggers, K., 1984, "The Utah/M.I.T. Dextrous Hand: Work in Progress," Int. J. Rob. Res., **3**(4), pp. 21–50.
[3] Salisbury, J. K., and Craig, J. J., 1982, "Articulated Hands: Force Control and Kinematic Issues," Int. J. Rob. Res., **1**(1), pp. 4–17.
[4] Lovchik, C. S., and Diftler, M. A., 1999, "The Robonaut Hand: A Dexterous Robot Hand for Space," IEEE International Conference on Robotics and Automation, Detroit, MI, May 10–15, pp. 907–912.
[5] Kochan, A., 2005, "Shadow Delivers First Hand," Ind. Rob. Int. J., **32**(1), pp. 15–16.
[6] Butterfass, J., Grebenstein, M., Liu, H., and Hirzinger, G., 2001, "DLR-Hand II: Next Generation of a Dextrous Robot Hand," IEEE International Conference on Robotics and Automation, Seoul, South Korea, May 21–26, pp. 109–114
[7] Speeter, T. H., 1991, "Primitive Based Control of the Utah/Mit Dextrous Hand," IEEE International Conference on Robotics and Automation, Sacramento, CA, Apr. 9–11, pp. 866–877.
[8] Xu, Z., Kumar, V., and Todorov, E., 2013, "A Low-Cost and Modular, 20-DOF Anthropomorphic Robotic Hand: Design, Actuation and Modeling," IEEE-RAS International Conference on Humanoid Robots (Humanoids), Atlanta, GA, Oct. 15–17, pp. 368–375.
[9] Deimel, R., and Brock, O., 2016, "A Novel Type of Compliant and Underactuated Robotic Hand for Dexterous Grasping," Int. J. Rob. Res., **35**(1–3), pp. 161–185.
[10] Tavakoli, M., Enes, B., Santos, J., Marques, L., and de Almeida, A. T., 2015, "Underactuated Anthropomorphic Hands: Actuation Strategies for a Better Functionality," Rob. Auton. Syst., **74**(pt. A), pp. 267–282.
[11] Dollar, A. M., and Howe, R. D., 2010, "The Highly Adaptive Sdm Hand: Design and Performance Evaluation," Int. J. Rob. Res., **29**(5), pp. 585–597.
[12] Laliberte, T., Birglen, L., and Gosselin, C., 2002, "Underactuation in Robotic Grasping Hands," J. Mach. Intell. Rob. Control, **4**(3), pp. 77–87.
[13] Birglen, L., 2009, "Type Synthesis of Linkage-Driven Self-Adaptive Fingers," ASME J. Mech. Rob., **1**(2), p. 021010.
[14] Zhang, C., Zhang, W., Sun, Z., and Zhen, Q., 2012, "Hag-sr Hand: Highly-Anthropomorphic-Grasping Under-Actuated Hand With Naturally Coupled States," International Conference on Social Robotics, pp. 475–484.
[15] Gosselin, C., Pelletier, F., and Laliberte, T., 2008, "An Anthropomorphic Underactuated Robotic Hand With 15 Dofs and a Single Actuator," IEEE International Conference on Robotics and Automation, Pasadena, CA, May 19–23, pp. 749–754.
[16] Li, X., Huan, Q., Yu, Z., Zhu, J., and Han, D., 2017, "A Novel Under-Actuated Bionic Hand and Its Grasping Stability Analysis," Adv. Mech. Eng., **9**(2), pp. 1–13.
[17] Liang, D., and Zhang, W., 2016, "A Novel Parallel and Self-Adaptive Underactuated Finger With Link-Wheel Mechanism," International Conference on Advanced Robotics and Mechatronics, Macau, China, Aug. 18–20, pp. 518–523.
[18] Luo, C., and Zhang, W., 2018, "A Flexible Self-Adaptive Underactuated Hand With Series Passive Joints," Ind. Rob. Int. J., **45**(4), pp. 516–525.
[19] Li, G., Li, B., Sun, J., Zhang, W., Sun, Z., and Chen, Q., 2013, "Development of a Directly Seld-Adaptive Robot Hand With Pulley-Belt Mechanism," Int. J. Precis. Eng. Manuf., **14**(8), pp. 1361–1368.
[20] Liang, D., Zhang, W., Sun, Z., and Chen, Q., 2015, "Pasa Finger: A Novel Parallel and Self-Adaptive Underactuated Finger With Pinching and Enveloping Grasp," IEEE Conference on Robotics and Biomimetics, Zhuhai, China, Dec. 6–9, pp. 1323–1328.
[21] Gao, B., Yang, S., Jin, H., Hu, Y., Yang, X., and Zhang, J., 2016, "Design and Analysis of Underactuated Robotic Gripper With Adaptive Fingers for Object Grasping Tasks," IEEE Conference on Robotics and Biomimetics, Qingdao, China, Dec. 3–7, pp. 987–992.
[22] Gao, B., Lei, L., Zhao, S., Hu, Y., and Zhang, J., 2016, "A Novel Underactuated Hand With Adaptive Robotic Fingers," IEEE International Conference on Information and Automation, Ningbo, China, Aug. 1–3, pp. 1392–1397.
[23] Birglen, L., 2017, "Design of a Partially-Coupled Self-Adaptive Robotic Finger Optimized for Collaborative Robots," Robotics: Science and Systems, Cambridge, MA, July 12–16, p. 9.
[24] Nunez-Altamirano, D. A., Juarez-Campos, I., Marquez-Parez, L., Flores-Diaz, O., and Romero-Munoz, L., 2016, "Dynamics of a Novel Robotic Leg Based on the Peaucellier-Lipkin Mechanism on Linear Paths During the Transfer Phase," Adv. Mech. Eng., **8**(7), pp. 1–10.
[25] Birglen, L., and Gosselin, C. M., 2004, "Kinetostatic Analysis of Underactuated Fingers," IEEE Trans. Rob. Autom., **20**(2), pp. 211–221.
[26] Belzile, B., and Birglen, L., 2015, "Instantaneous-Stiffness Plane Analysis of Underactuated Fingers," ASME Paper No. DETC2015-47310.
[27] Bai, S., and Angeles, J., 2008, "A Unified Input-Output Analysis of Four-Bar Linkages," Mech. Mach. Theory, **43**(2), pp. 240–251.
[28] Rothenhofer, G., Walsh, C., and Slocum, A., 2010, "Transmission Ratio Based Analysis and Robust Design of Mechanisms," Precis. Eng., **34**(4), pp. 790–797.
[29] Hunter, J. D., 2007, "Matplotlib: A 2D Graphics Environment," Comput. Sci. Eng., **9**(3), pp. 90–95.
[30] Sun, J., and Zhang, W., 2012, "A Novel Coupled and Self-Adaptive Under-Actuated Multi-Fingered Hand With Gear-Rack-Slider Mechanism," J. Manuf. Syst., **31**(1), pp. 42–49.